Chinese Chemical Letters 33 (2022) 4645–4648

Contents lists available at ScienceDirect

Chinese Chemical Letters

journal homepage: www.elsevier.com/locate/cclet

Nearly 100% exciton utilization in highly efficient red OLEDs based on dibenzothioxanthone acceptor

Xiaoxiao Hu[a,b], Yuanyuan Qin[a,b], Zhiyi Li[a,b], Honglei Gao[a,b], Teng Gao[a,b], Guanhao Liu[a,b], Xiangyu Dong[a,b], Naxi Tian[a,b], Xiuxian Gu[a,b], Chun-Sing Lee[c], Pengfei Wang[a,b], Ying Wang[a,b,*]

[a] Key Laboratory of Photochemical Conversion and Optoelectronic Materials and CityU–CAS Joint Laboratory of Functional Materials and Devices, Technical Institute of Physics and Chemistry, Chinese Academy of Sciences, Beijing 100190, China
[b] University of Chinese Academy of Sciences, Beijing 100049, China
[c] Center of Super-Diamond and Advanced Films (COSDAF), City University of Hong Kong, Hong Kong, China

ARTICLE INFO

Article history:
Received 30 September 2021
Revised 3 November 2021
Accepted 20 December 2021
Available online 24 December 2021

Keywords:
Red light
Organic light-emitting diode
Thermally activated delayed fluorescence
Exciton utilization
Locally excited triplet state

ABSTRACT

Improving the utilization of excitons has always been an important topic for the development of electroluminescence devices. In this work, we designed and synthesized three red TADF emitters TPA-DBT12, TPA-DBT3 and DTPA-DBT by employing dibenzothioxanthone (DBT) acceptor framework to stabilize the locally excited triplet state to participate in the reverse intersystem crossing (RISC) process. The fast RISC process and singlet radiation decay process gave rise to evidently enhanced exciton utilization. All of the red OLEDs based on these materials showed maximum EQE over 11% and high exciton utilization close to 100%. This work not only extend the acceptor framework for red materials but also provide a new perspective for the design of highly efficient red TADF materials with 100% exciton utilization by managing locally excited triplet state.

To date, organic light-emitting diodes (OLEDs) have been researched extensively because of the potential applications in flexible display and solid lighting [1–4]. Within such electroluminescence (EL) devices, 25% singlet excitons and 75% triplet excitons are generated by charge (hole and electron) recombination according to spin statistics [5,6]. Therefore, the harvest of triplet excitons is an important project for high-efficiency OLED devices. As the third-generation organic light-emitting materials, thermally activated delayed fluorescence (TADF) materials can theoretically achieve 100% triplet exciton harvest and thus 100% exciton utilization through effective up-conversion from triplet state to singlet state by minimizing the activated energy (ΔE_{ST}) between lowest triplet excited state (T_1) and singlet excited state (S_1) and develop rapidly [7–11].

OLEDs using TADF materials have achieved excellent results over 30% external quantum efficiency (EQE) with rapid reverse intersystem crossing (RISC) from T_1 to S_1 and strong radiation of singlet-to-ground state over the years [12–15], but their ability of harvesting triplet excitons is still unsatisfactory, especially for red TADF materials, so that their exciton utilization is generally low [16–20]. For example, Juan Qiao's group reported two linear TADF materials induced by J-aggregates with strong intermolecular charge transfer (CT), and the red OLEDs exhibit maximum external quantum efficiencies of 15.8% and 14.1% with nearly unity photoluminescence efficiency in solid films [19]. Obviously, the excitons generated by carrier recombination in the devices are not fully utilized. According to the energy gap law [21,22], as the band gap decreases, the non-radiative decay rate increases exponentially. In the development of red TADF materials, how to suppress non-radiative decay to increase the competitiveness of singlet radiation decay has been the focus of attention, while ignoring the importance of the up-conversion process by RISC from triplet to singlet. The result is that the aromatic and rigid structure is the first element to be considered when designing red materials, as lots of large conjugated acceptors of polycyclic aromatic hydrocarbons are often used to engineer molecules, like phenanthro[4,5-*abc*]phenazine-11,12-dicarbonitrile (PPDCN) [23], acenaphtho[1,2-*b*]quinoxaline-

* Corresponding author at: Key Laboratory of Photochemical Conversion and Optoelectronic Materials and CityU–CAS Joint Laboratory of Functional Materials and Devices, Technical Institute of Physics and Chemistry, Chinese Academy of Sciences, Beijing 100190, China.
E-mail address: wangy@mail.ipc.ac.cn (Y. Wang).

https://doi.org/10.1016/j.cclet.2021.12.047
1001-8417/

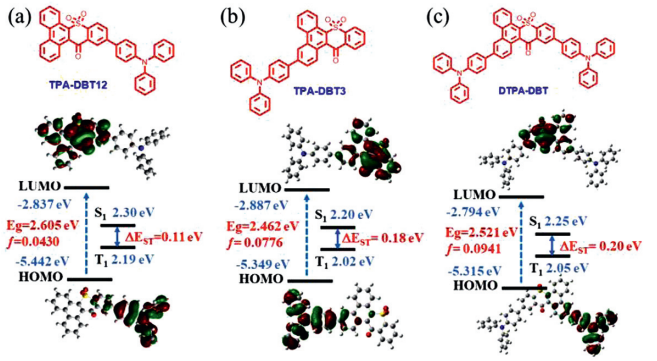

Fig. 1. Molecular structure, HOMO and LUMO electronic distributions, energy level, and bandgaps (E_g), the lowest singlet (S_1), and triplet (T_1) and oscillator strengths of S_1 (f) for (a) TPA-DBT12, (b) TPA-DBT3 and (c) DTPA-DBT calculated by TD-DFT at the b3lyp/6–31 g(d,p) level.

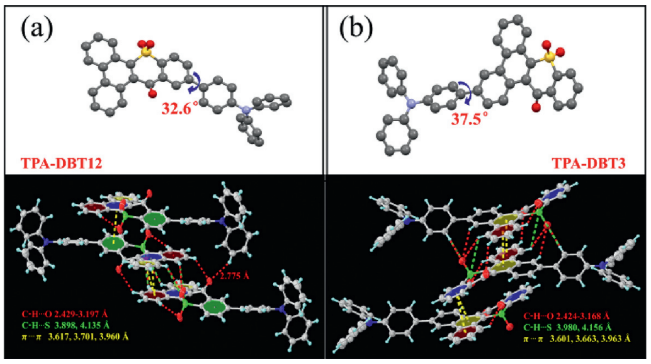

Fig. 2. Single crystal structure and molecular interactions of (a) TPA-DBT12 and (b) TPA-DBT3.

9,10-dicarbonitrile (ANQDC) [24], dibenzo[*a*,*c*]dipyrido[3,2-*h*:20,30-*j*]phenazine (BPPZ) [17], etc. Although their outstanding device performances with EQEs over 20% have been achieved, low exciton utilization due to triplet exciton loss caused by insufficient up-conversion process is still a problem for these materials.

The different nature of S_1 and T_1 states is found to strongly enhance spin-orbit coupling and promote the RISC according to the El-Sayed rule [25]. Thus, managing the locally excited triplet state (^{3}LE) to allow participation in the RISC process has become a common method to improve exciton utilization [26–28]. Herein, we successfully designed and synthesized three red TADF emitters TPA-DBT12, TPA-DBT3 and DTPA-DBT by employing an acceptor dibenzothioxanthone (DBT) framework to stabilize the locally excited triplet state. The fastest RISC rate could reach the order of 10^5 s^{-1} due to small ΔE_{ST} and enhanced spin-orbit coupling due to the involvement of ^{3}LE. And, the rate constants of singlet radiation decay reached the order of 10^7 s^{-1}, which further promoted the utilization of excitons. As a result, all of the red OLEDs based on these materials showed high EQE over 11% and exciton utilization close to 100%. This provides a new acceptor to improve exciton utilization by managing locally excited triplet state for highly efficient red TADF materials.

The synthesis and characterization of three red emitters were provided in Schemes S1 and S2 and Figs. S1–S3 (Supporting information). Excellent thermal stability with the decomposition temperatures (T_d) (the temperature at 5 wt% weight loss) and glass transition temperatures of 406.0 °C/128.4 °C for TPA-DBT12, 392.6 °C/128.0 °C for TPA-DBT3 and 485.5 °C/160.7 °C for DTPA-DBT were proved by thermal gravimetric analysis (TGA) and differential scanning calorimetry (DSC) under nitrogen atmosphere (Fig. S4 in Supporting information). Such good thermodynamic properties make them competent to general device fabrication and operation. The frontier orbital energy levels of the compounds were measured by cyclic voltammetry, as shown in Fig. S5 (Supporting information). Obviously, the changes in the position and number of the donor substitution had no effect on the LUMO energy level, all of them were −3.51 eV. Compared with TPA-DBT3 substituted at 3-position (HOMO of −5.35 eV), TPA-DBT12 substituted at 12-position had a deeper HOMO of −5.40 eV. Interestingly, asymmetric DTPA-DBT showed similar oxidation potential with TPA-DBT3, which is consistent with the theoretical calculation that the HOMO of DTPA-DBT is mainly dispersed on the TPA at 3-position (Fig. 1), implying that the photophysical properties of the ground state were similar to that of TPA-DBT3. In addition, for all emitters, the effective HOMO-LUMO separation, more specifically, their LUMOs were localized on the DBT units and their HOMOs were mainly distributed in the TPA units and extended to the benzene ring of the DBT helps to achieve a small ΔE_{ST} and a large oscillator strength (f) [29–32], as shown in Fig. 1, and all the results are summarized in Table S1 (Supporting information).

Single-crystal X-ray structure analysis was carried out to further understand the influence of the substitution position of DBT receptor on molecular structure and stacking mode (Fig. 2). The similar dihedral angles between donor and acceptor were observed: 32.6° for TPA-DBT12 and 37.5° for TPA-DBT3 respectively. Such proper dihedral angles can not only ensure the effective separation of the frontier orbital, but also help to facilitate the expansion of the conjugation. Interestingly, similar short contacts and π–π interactions among the molecules can be observed. These multiple short interactions and efficient $\pi\cdots\pi$ stacking help to lock the molecular conformation, largely reducing the loss *via* non-radiative relaxation and thus affording the high fluorescence quantum yields (Φ_{PL}) in solid [33–35]. The difference is that for TPA-DBT12, the hydrogens at positions 4 and 5 of the phenanthrene ring were fixed by two short intermolecular contacts *via* C—H···O and C—H···S, while only the hydrogen at position 5 of TPA-DBT3 had such a connection. Additionally, the short interaction of C—H···O with 2.775 Å between the carbonyl group and the benzene ring of TPA from non-adjacent molecule can also be observed for TPA-DBT12. Such tight interaction supports TPA-DBT12 with better thermodynamic stability. Furthermore, as can be seen from Fig. S6 (Supporting information), TPA-DBT3 formed a columnar stacking along the crystallographic *b*-axis direction, affording a large intermolecular π-overlap, what could explain its higher Φ_{PL} in solid film. However, TPA-DBT12 stacked tightly by a sandwiched structure offering a charge-transfer pathway and enhancing the mobility, which was essential for excellent electroluminescence materials [36,37].

Photophysical properties of three compounds were investigated using ultraviolet-visible (UV–vis) and photoluminescence (PL) spectrometer and the results were summarized in Table S1. In solutions, the absorption spectra for all compounds exhibited a broad, featureless absorption band with 400~500 nm (Fig. S7a in Supporting information), which was defined as intramolecular CT absorption. With the increase of solvent polarity from *n*-hexane to 1,4-dioxane, their absorption spectra had no obvious change, however, a significant red shift was observed in their emission spectra (Fig. S7b in Supporting information). Especially for TPA-DBT12, which exhibited LE emission with fine structure in n-hexane (peak at 502 nm), and CT emission with featureless structure in 1,4-dioxane (peak at 622 nm). Such obvious characteristic of intramolecular CT provides the possibility to realize E-type delayed fluorescence. The ΔE_{ST} of 0.06 eV for TPA-DBT12, 0.17 eV for TPA-DBT3 and 0.17 eV for DTPA-DBT can be obtained according to the onset of fluorescence spectra at room temperature and phospho-

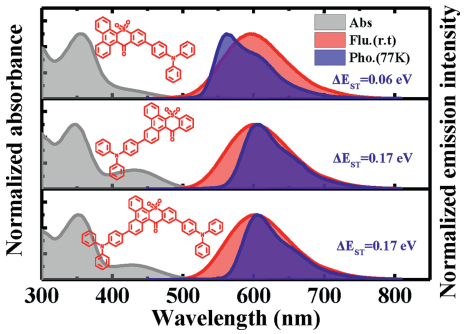

Fig. 3. Normalized UV–vis absorption spectra, fluorescence and phosphorescence spectra of TPA-DBT12, TPA-DBT3 and DTPA-DBT in toluene.

rescence spectra at 77 K (Fig. 3), which are sufficiently small to induce TADF characteristics. It is interesting to observe that all phosphorescence spectra showed obvious LE characteristic with fine structure, and the substitution of 3-position for DBT induces the lowest energy level of T_1. As a result, compared with TPA-DBT12 and DBT, the phosphorescence emissions of TPA-DBT3 and DTPA-DBT in toluene are red-shifted (Fig. S8 in Supporting information), which are consistent with the results by theoretical calculation for the natural transition orbitals (NTOs) (Figs. S9–S11 in Supporting information). For the T_1 state of TPA-DBT12, the overlap of hole and particle distributed in the heterocycle and benzene ring attached to the donor suggests the possibility with LE characteristics. And the large overlap focused on phenanthrene segment between hole and particle NTOs of T_1 states for TPA-DBT3 and DTPA-DBT also verifies the characteristics of their mainly local-excited triplet state. In addition, the SOC matrix element values between S_1 and T_1 were calculated as 0.27, 0.33, 0.55 cm^{-1} for TPA-DBT12, TPA-DBT3 and DTPA-DBT, respectively. Thus, these results indicate that the locally excited triplet state is allowed participation in the RISC process for three emitters.

Due to the strong aggregation-caused quenching of the compounds, the fluorescence spectra cannot be detected in pure film, so we dispersed them with doping concentration of 5% into the 3,5-bis(3-(9*H*-carbazol-9-yl)phenyl)pyridine (35DCzPPY), a host material with high T_1/S_1 to confine the excitons on guest molecules. All doped films gave red photoluminescence spectra with peak at 597 nm for TPA-DBT12, 616 nm for TPA-DBT3 and 632 nm for DTPA-DBT and high PLQYs of 45.3% for TPA-DBT12, 52.9% for TPA-DBT3, and 39.1% for DTPA-DBT under a nitrogen atmosphere. Furthermore, the PLQYs increased by 2%–8% in vacuum (Fig. S12 in Supporting information), indicating the contribution of triplet excitons to luminescence (the triplet oxygen in the air has a quenching effect on the triplet excitons of the materials), which further proved the possibility of possessing TADF properties [38].

Transient photophysical testing can serve as the most convincing manner to evaluate the performance of TADF. As can be seen from Fig. 4, all of the doped films show clear second-order exponential decays both prompt and delayed components with lifetimes of 9 ns/21.7 μs for TPA-DBT12, 11 ns/241.1 μs for TPA-DBT3, and 8 ns/70.3 μs for DTPA-DBT, and PL spectra of both components match very well (Figs. 4d-f). There is no obvious temperature dependence for their prompt lifetimes corresponding to the direct S_1 relaxation to S_0 (Fig. S13 in Supporting information), while the proportion of the delay component decreases as the temperature decreases (Figs. 4a-c), thence demonstrating the radiative decay of S_1 state via an up-conversion from triplet state to the singlet state, which is in line with the traditional TADF materials [29,39–42]. Their key kinetic parameters are summarized in Table 1. Surprisingly, all the rate constants of singlet radiation decay (k_r^S) are of the order of 10^7 s^{-1}, in detail, the maximum value of 3.45 × 10^7 s^{-1} for TPA-DBT3 corresponds to higher oscillator strength of 0.078, while, the k_r^S for DTPA-DBT with the highest oscillator strength of 0.094 is slightly weaker than that of TPA-DBT3 due to the serious non-radiative decay at long wavelength, which not only explains the high fluorescence quantum yield of these red materials, but also provides indirect support for the rapid RISC process. Their different RISC process greatly leads to their different exciton utilizations, TPA-DBT12 has the fastest reverse intersystem crossing constant (1.17 × 10^5 s^{-1}) mainly due to its relatively small ΔE_{ST}. While, DTPA-DBT, which has similar ΔE_{ST} and ^{3}LE characteristic with TPA-DBT3, exhibits faster k_{RISC}, and the possible reason is that the spin-orbit coupling between S_1 and T_1 is stronger (0.55 cm^{-1}) than that of TPA-DBT3 (0.33 cm^{-1}). Thus, more efficient triplet utilizations for TPA-DBT12 and DTPA-DBT can be obtained.

To evaluate the electroluminescence properties of three emitters, multilayer OLED devices were fabricated. The device architecture, molecular structures and energy levels were shown in Fig. S14 (Supporting information), and the electroluminescent characteristics of the devices are shown in Fig. 5 and summarized in Ta-

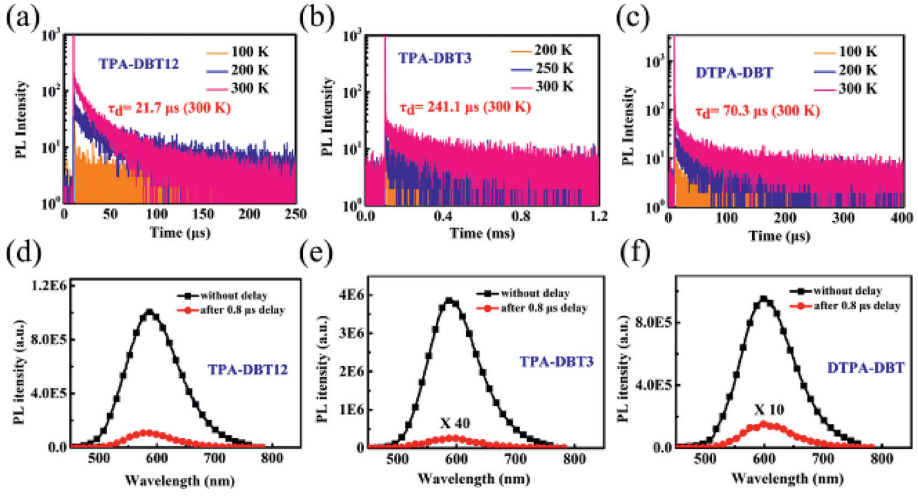

Fig. 4. Temperature-dependence of the transient PL spectra of doped films: (a) TPA-DBT12, (b) TPA-DBT3 and (c) DTPA-DBT and PL spectra of doped films at 300 K without delay and with a delay of 0.8 μs: (d) TPA-DBT12, (e) TPA-DBT3 and (f) DTPA-DBT. The doping ratio of all doped films is 5%.

Table 1
The summary of computing transient characterization in doped films.

Sample	τ_s (ns)	τ_d (μs)	Φ_{total} (%)	Φ_{prompt} (%)	Φ_{TADF} (%)	Φ_T (%)	k_p (s^{-1})	k_{ISC} (s^{-1})	k_r^s (s^{-1})	k_{nr}^s (s^{-1})	k_{RISC} (s^{-1})
TPA-DBT12	9	21.7	44.70	17.64	27.06	60.54	1.11×10^8	6.72×10^7	1.96×10^7	2.42×10^7	1.17×10^5
TPA-DBT3	11	241.1	55.50	38.00	17.50	31.57	9.09×10^7	2.87×10^7	3.45×10^7	2.77×10^7	6.05×10^3
DTPA-DBT	8	70.3	42.10	26.27	15.83	37.68	1.25×10^8	4.71×10^7	3.28×10^7	4.51×10^7	2.27×10^4

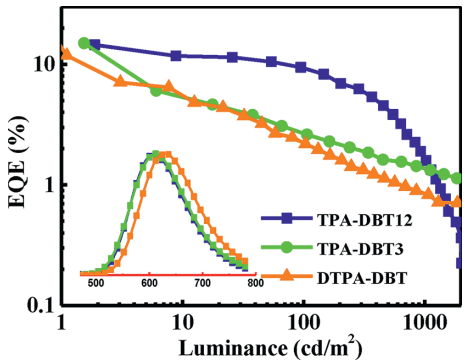

Fig. 5. EQE–luminance characteristics of the devices with the structure of ITO (95 nm)/α-NPD (15 nm)/TCTA (5 nm)/mCP (5 nm)/35DCzPPY: 5% emitters (30 nm)/B4PYMPM (70 nm)/LiF (1.1 nm)/Al (100 nm). Insert: EL spectra.

ble S2 (Supporting information). All of the devices can be turned on at 2.5–2.8 V, and the electroluminescence spectra with emission peak at 608 nm for TPA-DBT12, 612 nm for TPA-DBT3, and 628 nm for DTPA-DBT were similar with corresponding PL spectra. The maximum EQE reached 14.5% for TPA-DBT12, 15.0% for TPA-DBT3 and 11.8% for DTPA-DBT, and the maximum power efficiency (PE) and current efficiency (CE) are 28.9 lm/W, 25.8 cd/A for TPA-DBT12, 31.1 lm/W, 26.2 cd/A for TPA-DBT3 and 16.6 lm/W, 14.8 cd/A for DTPA-DBT respectively, which has a certain competitiveness in the red emission region (Fig. S16 and Table S3 in Supporting information). Furthermore, the efficiency roll-off of the device based on TPA-DBT12 is significantly lower than the others due to shorter delayed fluorescence lifetime of 21.7 μs, and the EQE can be as high as 9.3% at the luminescence up to 100 cd/m^2. It is worth noting that high exciton utilization efficiencies of near 100% for TPA-DBT12 and DTPA-DBT and 94.5% for TPA-DBT3 can be achieved when the fluorescence quantum yields of doped films (45.3% for TPA-DBT12, 52.9% for TPA-DBT3 and 39.1% for DTPA-DBT) were considered and the output-coupling efficiency of 30% was assumed. These results indicate that almost 100% triplet excitons for this series of emitters can be harvested through efficient RISC. Thus, excellent red OLED devices were realized successfully.

In conclusion, we designed and synthesized three red TADF emitters TPA-DBT12, TPA-DBT3 and DTPA-DBT by employing DBT acceptor framework. The natural transition orbitals (NTOs) and phosphorescence spectra verified the characteristics of their locally excited triplet states. Especially for TPA-DBT12, it possessed the fastest RISC rate on the order of 10^5 s^{-1} due to its relatively small ΔE_{ST} and enhanced spin-orbit coupling due to the involvement of ^{3}LE. The red OLEDs based on these materials showed maximum EQE of 14.5% with EL peak at 608 nm for TPA-DBT12, 15.0% with EL peak at 612 nm for TPA-DBT3 and 11.8% with EL peak at 628 nm for DTPA-DBT. Particularly, the exciton utilizations can reach to 100% for TPA-DBT12 and DTPA-DBT, even if low fluorescence quantum yield: 45.3% for TPA-DBT12 and 39.1% for DTPA-DBT. Our work provides a new acceptor to improve exciton utilization by managing locally excited triplet state for the highly efficient red TADF materials.

Declaration of competing interest

The authors declare that they have no known competing financial interests or personal relationships that could have appeared to influence the work reported in this paper.

Acknowledgments

This work was financially supported by the National Natural Science Foundation of China (No. 21772209) and the National Program for Support of Top-notch Young Professionals.

Supplementary materials

Supplementary material associated with this article can be found, in the online version, at doi:10.1016/j.cclet.2021.12.047.

References

[1] S. Kim, H.J. Kwon, S. Lee, et al., Adv. Mater. 23 (2011) 3511–3516.
[2] H. Sasabe, J. Kido, J. Mater. Chem. C 1 (2013) 1699.
[3] R. Kataishi, T. Ikeda, T. Sasaki, et al., J. Soc. Inf. Disp. 22 (2014) 381–392.
[4] G. Hong, X. Gan, C. Leonhardt, et al., Adv. Mater. 33 (2021) 2005630.
[5] M. Pope, H.P. Kallmann, P. Magnante, J. Chem. Phys. 38 (1963) 2042–2043.
[6] M.A. Baldo, D.F. O'Brien, Y. You, et al., Nature 395 (1998) 151–154.
[7] H. Wang, X. Lv, L. Meng, et al., Chin. Chem. Lett. 29 (2018) 471–474.
[8] W. Chen, F. Song, Chin. Chem. Lett. 30 (2019) 1717–1730.
[9] H. Nakanotani, Y. Tsuchiya, C. Adachi, Chem. Lett. 50 (2021) 938–948.
[10] Q. Xue, G. Xie, Adv. Opt. Mater. 9 (2021) 2002204.
[11] Y.J. Yu, X.Q. Wang, J.F. Liu, et al., Science 24 (2021) 102123.
[12] H. Kaji, H. Suzuki, T. Fukushima, et al., Nat. Commun. 6 (2015) 8476.
[13] T.A. Lin, T. Chatterjee, W.L. Tsai, et al., Adv. Mater. 28 (2016) 6976–6983.
[14] Z. Li, D. Yang, C. Han, et al., Angew. Chem. Int. Ed. 60 (2021) 14846–14851.
[15] Y.Y. Wang, K.N. Tong, K. Zhang, et al., Mater. Horiz. 8 (2021) 1297–1303.
[16] Q. Zhang, H. Kuwabara, W.J. Potscavage, et al., J. Am. Chem. Soc. 136 (2014) 18070–18081.
[17] J.X. Chen, K. Wang, C.J. Zheng, et al., Adv. Sci. 5 (2018) 1800436.
[18] R. Furue, K. Matsuo, Y. Ashikari, et al., Adv. Opt. Mater. 6 (2018) 1701147.
[19] J. Xue, Q. Liang, R. Wang, et al., Adv. Mater. 31 (2019) 1808242.
[20] M. Yang, I.S. Park, T. Yasuda, J. Am. Chem. Soc. 142 (2020) 19468–19472.
[21] R. Englman, J. Jortner, Mol. Phys. 18 (1970) 145–164.
[22] J.V. Caspar, E.M. Kober, B.P. Sullivan, et al., J. Am. Chem. Soc. 104 (1982) 630–632.
[23] T. Yang, Z. Cheng, Z. Li, et al., Adv. Funct. Mater. 30 (2020) 2002681.
[24] X. Gong, P. Li, Y.H. Huang, et al., Adv. Funct. Mater. 30 (2020) 1908839.
[25] M.A. El Sayed, J. Chem. Phys. 38 (1963) 2834–2838.
[26] P.K. Samanta, D. Kim, V. Coropceanu, et al., J. Am. Chem. Soc. 139 (2017) 4042–4051.
[27] J.X. Chen, Y.F. Xiao, K. Wang, et al., Angew. Chem. Int. Ed. 60 (2021) 2478–2484.
[28] D. Karthik, Y.H. Jung, H. Lee, et al., Adv. Mater. 33 (2021) 2007724.
[29] H. Uoyama, K. Goushi, K. Shizu, et al., Nature 492 (2012) 234–238.
[30] S. Hirata, Y. Sakai, K. Masui, et al., Nat. Mater. 14 (2015) 330–336.
[31] Y. Im, M. Kim, Y.J. Cho, et al., Chem. Mater. 29 (2017) 1946–1963.
[32] W. Yuan, H. Yang, M. Zhang, et al., Chin. Chem. Lett. 30 (2019) 1955–1958.
[33] H. Liu, L. Yao, B. Li, et al., Chem. Commun. 52 (2016) 7356–7359.
[34] S.K. Mohan Nalluri, J. Zhou, T. Cheng, et al., J. Am. Chem. Soc. 141 (2019) 1290–1303.
[35] Y. Shen, Z. Zhang, H. Liu, et al., J. Phys. Chem. C 123 (2019) 13047–13056.
[36] K. Wang, F. Zhao, C. Wang, et al., Adv. Funct. Mater. 23 (2013) 2672–2680.
[37] H. Wang, L. Xie, Q. Peng, et al., Adv. Mater. 26 (2014) 5198–5204.
[38] G. Méhes, H. Nomura, Q. Zhang, et al., Angew. Chem. Int. Ed. 51 (2012) 11311–11315.
[39] H. Tanaka, K. Shizu, H. Miyazaki, et al., Chem. Commun. 48 (2012) 11392.
[40] F.B. Dias, K.N. Bourdakos, V. Jankus, et al., Adv. Mater. 25 (2013) 3707–3714.
[41] S.Y. Lee, C. Adachi, T. Yasuda, Adv. Mater. 28 (2016) 4626–4631.
[42] P. Rajamalli, N. Senthilkumar, P. Gandeepan, et al., J. Am. Chem. Soc. 138 (2016) 628–634.